Analytical modeling and x-ray imaging of oscillations of a single magnetic domain wall

Lars Bocklage,[1,*] Benjamin Krüger,[2,†] Peter Fischer,[3] and Guido Meier[1]
[1]*Institut für Angewandte Physik und Zentrum für Mikrostrukturforschung, Universität Hamburg, Jungiusstrasse 11, 20355 Hamburg, Germany*
[2]*I. Institut für Theoretische Physik, Universität Hamburg, Jungiusstrasse 9, 20355 Hamburg, Germany*
[3]*Center for X-Ray Optics, Lawrence Berkeley National Laboratory, 1 Cyclotron Road, Berkeley, California 94720, USA*
(Received 17 June 2009; published 4 February 2010)

Domain wall oscillation in a pinning potential is described analytically in a one-dimensional model for the field-driven case. A proper description of the pinning potential has to go beyond harmonic contributions. Oscillations of a domain wall are observed by time-resolved magnetic soft x-ray microscopy. It is shown that nonharmonic terms are present in real samples with a strong restoring potential. In the framework of our model we gain deep insight into the domain wall motion by looking at different phase spaces. The corrections of the harmonic potential can change the motion of the domain wall significantly. The damping parameter of permalloy is determined via the direct imaging technique.

DOI: 10.1103/PhysRevB.81.054404 PACS number(s): 75.60.Ch, 68.37.Yz, 85.75.−d, 76.50.+g

I. INTRODUCTION

Magnetization patterns with single elementary magnetic structures, such as vortices or domain walls, form on the micro and nanometer scale. Their magnetization dynamics occur on the nanosecond and picosecond time scale. Both size and speed of these patterns are of great interest in today's research for prospective nonvolatile data storage devices.[1–3] These magnetization structures are coupled locally via the exchange interaction and globally via the magnetic stray field. Nonetheless, an analytical description of their dynamics is possible.[4,5] The motion of the magnetization can be excited by magnetic fields or currents and both can be included in the analytical description.[6,7] The motion of a domain wall along a nanowire can be caused by current via the spin torque[8–10] or by its Oersted field.[11,12] However, the clear distinction of these two different effects is not simple.[13] In the case of vortices or domain walls in confining potentials the identification of the driving force is even more complicated. Spatially and temporally resolved experimental methods are needed. One possible tool is magnetic transmission x-ray microscopy, which provides a spatial resolution down to 15 nm[14] and a temporal resolution below 100 ps.[15] Hence, this method matches the requirements to study magnetization dynamics down to fundamental magnetic length and time scales.

In this work we study analytically and experimentally the dynamics of a confined magnetic domain wall. Some results of Ref. 11 are repeated for better comprehension and are reviewed with the present analytical tools. Subsequently we give a detailed analysis of the domain wall oscillations. The work is organized as follows. After the introduction we focus in the second part on the analytical description of field-induced oscillations of a single domain wall. An analytical solution of the Landau-Lifshitz-Gilbert equation is deduced. In Sec. III the experimental setup used to image domain wall oscillations is described. In the fourth part we present results of time-resolved x-ray microscopy and its analytical description. We show that a simple harmonic oscillator model cannot describe the dynamics of the wall. Higher-order terms are required to describe the confining potential of the domain wall in the experiments. The influence of the nonharmonic contributions on the out-of-plane tilting of the domain wall is studied analytically. This tilting can be compared with the velocity of the domain wall. So far, the damping parameter of permalloy has been intensively studied with ferromagnetic resonance or with Kerr microscopy.[16–21] We determine the damping parameter by directly imaging the motion of the magnetization with time-resolved soft x-ray microscopy. Section V gives a conclusion.

II. MICROMAGNETIC MODEL

The Landau-Lifshitz-Gilbert (LLG) equation,

$$\frac{d\vec{M}}{dt} = -\gamma\vec{M}\times\vec{H}_{\mathrm{eff}} + \frac{\alpha}{M_S}\vec{M}\times\frac{d\vec{M}}{dt}, \tag{1}$$

describes the dynamics of the magnetization $\vec{M}$. Here, $\vec{H}_{\mathrm{eff}}$, γ, α, and M_S denote the effective magnetic field, the gyromagnetic ratio, the Gilbert damping parameter, and the saturation magnetization, respectively. The domain wall dynamics are implicated by the LLG equation and can be described analytically with the assumption of a rigid domain wall.[22] The equations of motion have been derived in Ref. 6. We neglect the current-induced terms of the dynamics and obtain the equations of motion for the center of the wall Y and the angle of the rotation of the wall out-of-plane ϕ. The equations are

$$\dot{Y} = -\frac{2\lambda\gamma' K_\perp}{\mu_0 M_S}\phi - \lambda\gamma'\alpha H(Y), \tag{2}$$

and

$$\dot{\phi} = \gamma' H(Y) - \frac{2\gamma'\alpha K_\perp}{\mu_0 M_S}\phi, \tag{3}$$

with $\gamma' = \gamma/(1+\alpha^2)$ and the domain wall width $\lambda = \sqrt{A/K}$. A is the exchange constant and K is the anisotropy constant for

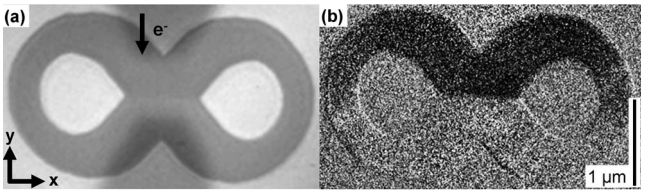

FIG. 1. (a) X-ray image of the investigated sample showing the permalloy structure and the gold contacts. The electron flow is indicated by an arrow. (b) Static differential image obtained from an image at remanence and an image at saturation. It shows the altered magnetization in the upper part of the structure at remanence (black) in contrast to the saturated state. Therefore the magnetization of the black part has reversed and a 180° domain wall has formed at the intersection in the center.

the magnetization pointing in the y direction, while $K+K_\perp$ is the anisotropy for the magnetization pointing out-of-plane. The in-plane magnetic field H consists of the external field H_{ext} and the pinning field H_{pin}. Both point in x direction, i.e., perpendicular to the current which flows in y direction. The coordinate system is given in Fig. 1. In the time derivative of Eq. (2) $\dot{\phi}$ is replaced by the right-hand side of Eq. (3) which yields

$$\ddot{Y} = -\frac{2\lambda\gamma'^2 K_\perp}{\mu_0 M_S}\left(H(Y) - \frac{2\alpha K_\perp}{\mu_0 M_S}\phi\right) - \lambda\gamma'\alpha\dot{H}(Y). \quad (4)$$

Solving Eq. (2) for the angle

$$\phi = -\frac{\mu_0 M_S}{2K_\perp}\left(\frac{1}{\gamma'\lambda}\dot{Y} + \alpha H(Y)\right), \quad (5)$$

and inserting this expression in Eq. (4) yields the following relation for the position of the domain wall

$$\ddot{Y} = -\frac{\lambda\gamma H(Y) + \alpha\dot{Y}}{\alpha\tau_d} - \lambda\gamma'\alpha\dot{H}(Y). \quad (6)$$

The damping time τ_d, in which the free wall slows down to e^{-1} of its initial velocity, is given by

$$\tau_d = \frac{\mu_0 M_S}{2\gamma'\alpha K_\perp}. \quad (7)$$

The energy of the domain wall is derived by solving the energy functional given in Ref. 6 which is extended by the pinning energy

$$E = \int\left[\frac{2K}{\cosh^2\left(\frac{y-Y}{\lambda}\right)} + \frac{A}{\cosh^2\left(\frac{y-Y}{\lambda}\right)}\left(\frac{\partial\phi}{\partial y}\right)^2\right]dV + \int\left[\frac{K_\perp\phi^2}{\cosh^2\left(\frac{y-Y}{\lambda}\right)} - \mu_0 M_S H_{\mathrm{ext}}(y)\tanh\left(\frac{y-Y}{\lambda}\right)\right]dV + E_{\mathrm{pin}}(Y). \quad (8)$$

We neglect all constant contributions, i.e., terms that do not depend on Y or ϕ. If the external field is spatial homogeneous the energy of the domain wall is given by

$$E = 2S\lambda K_\perp\phi^2 + 2S\mu_0 M_S Y H_{\mathrm{ext}} + E_{\mathrm{pin}}(Y), \quad (9)$$

with the S being the geometrical cross section of the structure. The pinning field is given in Ref. 23 and reads

$$H_{\mathrm{pin}} = \frac{1}{2S\mu_0 M_S}\frac{dE_{\mathrm{pin}}}{dY}. \quad (10)$$

As the field is $H(y)=H_{\mathrm{ext}}(y)+H_{\mathrm{pin}}(y)$ we calculate the reaction of the domain wall on the pinning field from Eq. (6). The time derivative of the pinning field is small and can be neglected. We get

$$\ddot{Y}_{\mathrm{pin}} = -\frac{\lambda\gamma'^2 K_\perp(1+\alpha^2)}{S\mu_0^2 M_S^2}\frac{dE_{\mathrm{pin}}}{dY} = -\frac{1+\alpha^2}{m}\frac{dE_{\mathrm{pin}}}{dY}. \quad (11)$$

The domain wall mass m is defined in Ref. 6

$$m = \frac{S\mu_0^2 M_S^2}{\lambda\gamma'^2 K_\perp} = \frac{2\alpha S\mu_0 M_S\tau_d}{\lambda\gamma'}. \quad (12)$$

With this definition of the mass the kinetic energy of the wall $\frac{1}{2}m\dot{Y}$ can be calculated for a stationary motion without magnetic fields. Interestingly, the mass of the domain wall differs by a factor of $(1+\alpha^2)^{-1}$ to satisfy the equations of motion. Consequently a different mass $m'=\frac{m}{1+\alpha^2}$ determines the reaction of the wall on magnetic fields. As the damping parameter in permalloy is small the difference is negligible. However, in strongly damped systems this effect should be more pronounced. Equation (6) becomes

$$\ddot{Y} = -\frac{\lambda\gamma H_{\mathrm{ext}} + \alpha\dot{Y}}{\alpha\tau_d} - \lambda\gamma'\alpha\dot{H}_{\mathrm{ext}} - \frac{1}{m'}\frac{dE_{\mathrm{pin}}}{dY}. \quad (13)$$

In addition to the exciting field, the material parameters and the shape of the sample the dynamics of the domain wall also depend linearly on the width of the wall itself.

Oscillations of a single domain wall are characterized by the confining potential E_{pin}. In a first approximation a harmonic potential

$$E_{\mathrm{pin}} = \frac{1}{2}m'\omega_r^2 Y^2, \quad (14)$$

with the resonance frequency ω_r is used to describe these oscillations. However, deviations from the harmonic potential can occur in a real sample depending on its size and shape.[11,24] In this case nonharmonic terms have to be added to the potential which can be evolved into the power series

$$E_{\mathrm{pin}} = \sum_{n=1}^{\infty}\frac{1}{2n}m' k_n Y^{2n}. \quad (15)$$

Equation (14) is obtained if $k_1=\omega_r^2$ and all constants of the higher order terms are small compared to k_1. As shown by time-resolved x-ray imaging of the oscillations of a single domain wall described in Sec. IV these deviations occur and at least the first correction terms to the harmonic potential can be significant.

In the following part of this section we show how the damping parameter can be derived from the damping time and the domain wall width. The anisotropy in y direction can be calculated from the domain wall width as

$$K = \frac{A}{\lambda^2}. \tag{16}$$

The sum of all three magnetic anisotropy constants is given by

$$K_x + K_y + K_z = 2K + K_\perp = \frac{1}{2}\mu_0 M_S^2 \tag{17}$$

since the anisotropy is given by the dipolar field alone. Insertion of Eq. (16) in Eq. (17) yields the value of the perpendicular anisotropy

$$K_\perp = \frac{1}{2}\mu_0 M_S^2 - 2\frac{A}{\lambda^2}. \tag{18}$$

Inserting this result in Eq. (7) allows to determine the damping parameter

$$\alpha = x - \sqrt{x^2 - 1} \quad \text{with} \quad x = \frac{\gamma\tau_d(\mu_0 M_S^2 - 4A/\lambda^2)}{2\mu_0 M_S}. \tag{19}$$

While the values for the saturation magnetization, the gyromagnetic ratio, and the exchange constant are known, the damping time and the domain wall width can be directly determined from the experimental data.

III. EXPERIMENTAL SETUP

Time-resolved soft x-ray microscopy was performed at beamline 6.1.2 at the Advanced Light Source in Berkeley, CA. This full-field soft x-ray transmission microscope provides magnetic contrast by the x-ray magnetic circular dichroism.[25] In the present measurements Fresnel zone plates provide a spatial resolution of 25 nm. A stroboscopic pump-and-probe measurement scheme provides a temporal resolution below 100 ps.[11] Due to the transmission design of the microscope the microstructures have to be prepared on 100–nm-thin Si_3N_4 membranes. Electron-beam lithography, thermal evaporation, and lift-off processing techniques are used to prepare the 20-nm-thin permalloy ($Ni_{80}Fe_{20}$) structure shown in Fig. 1(a). The structure is contacted by wave guides fabricated by electron-beam lithography, dc-magnetron sputtering of 2 nm Al and 20 nm Au, and lift-off processing.

To enhance the magnetic contrast two x-ray images are illuminated at both a magnetically saturated state and at remanence. These two images are then divided and one obtains a grayscale image where the changes of the local magnetization relative to the saturated state show up as dark or bright contrast [see Fig. 1(b)]. The time-resolved images are normalized to an image taken before the excitation has started, i.e., without dynamics, which is typically the first image in a time scan ($t=0$). Hereby the change in the magnetization at times $t>0$ is detected by a changing contrast. Time scans covering a total of 6 ns time delay between the electronic pump pulse and the x-ray probe pulse in steps of 200 ps were recorded.

IV. RESULTS

Figure 1(a) shows the investigated "infinity" shaped structure used for this study. After being completely saturated along the $-x$ direction in a field of $\sim$50 mT the external field is set to zero. The magnetic configuration obtained by this initialization procedure is shown in Fig. 1(b). The upper and lower parts in the structure are magnetized in opposite directions and therefore a 180° domain wall is located in between. The tip-shaped holes of the structure are pinning sites for the domain wall by minimizing the domain wall length and energy. Therefore the domain wall is confined in a restoring potential.

The domain wall is excited by current pulses flowing in y direction through the ferromagnetic structure. The current density is $5\cdot10^{11}$ A/m^2. The current flows directly through the structure in contrast to experiments where an Oersted field of a strip line is used as a source for radio frequency field excitation. Nonetheless, in the present experiments the main source of excitation is not spin-torque but the current's Oersted field. The exciting force is discussed in detail in Ref. 11. The important point for the present study is that a short magnetic field pulse in x direction excites the domain wall oscillation. Then the dynamics of the domain wall can be described by the model presented in Sec. II. The field pulse has the same time structure as the current pulse.

Dynamic differential images showing the domain wall dynamics are presented in Fig. 2(a) for different delay times with a field pulse length of 1.1 ns. The white and black contrast indicates the vertical motion of the domain wall up and down, respectively. Figure 2(b) shows the progress of the maximal vertical deflection of the domain wall in y direction for different pulse lengths. The domain wall is deflected as long as the current pulse is applied and oscillates around the deflected position. Afterwards the domain wall performs a free damped oscillation. The domain wall is pinned at the ends and it bows during its motion. The maximum deflection is used as its position Y. The bending is not included in the model as it assumes a rigid particle. The aspect ratio of the maximum deflection in y direction and its length in x direction is only 0.1 and the discrepancy to the assumption is therefore small.

To extract the potential of the domain wall the free oscillation is fitted to

$$Y(t) = Ae^{-\Gamma(t-t_0)}\cos\,\omega(t-t_0), \tag{20}$$

for the current pulses of 1.1 ns duration. The fit to the experimental data is shown in Fig. 2 as dashed green line. One derives the following parameters from the fit: the amplitude $A=125$ nm, the damping constant $\Gamma=554$ MHz, the start time of the free oscillation $t_0=1.85$ ns, and the free angular frequency $\omega=3.6$ GHz. For the frequency of the free oscillation one obtains $f=573$ MHz and a damping time $\tau_d=(2\Gamma)^{-1}$ of 0.9 ns. The resonance frequency is given by $\omega_r=\sqrt{\omega^2+\Gamma^2}$. This simple model is adequate as long as the deflection of the domain wall is small and the restoring force is determined by a harmonic potential. We will see that the harmonic part of the total potential is well described with these parameters.

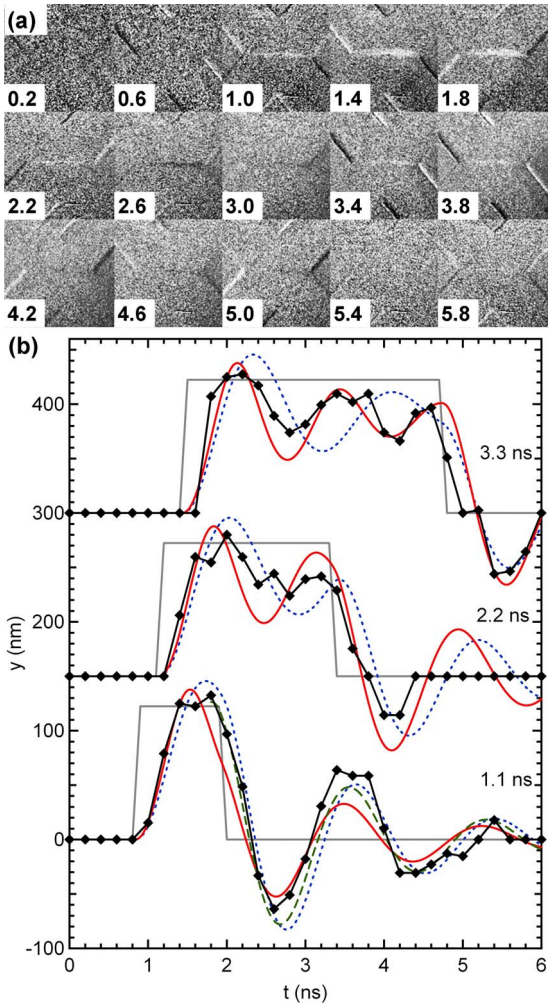

FIG. 2. (Color online) (a) Dynamic differential images for the inner section of the structure for different time steps indicated by the lower left number in units of nanoseconds. The pulse length is 1.1 ns. (b) Progress of the maximal vertical deflection of the domain wall (diamonds) for pulse lengths of 1.1, 2.2, and 3.3 ns. The curve offset for 2.2 ns (3.3 ns) is 150 nm (300 nm) for clarity. The black lines are guides to the eye. The gray lines depict the time structure of the current pulses. The dashed green curve is a fit to the free damped oscillation using Eq. (20) for a pulse width of 1.1 ns. The dotted blue and solid red lines are fits to the integration of Eq. (13) with a harmonic and a nonharmonic potential, respectively.

With Eq. (13) the entire time evolution of the domain wall position can be fitted. The domain wall position is calculated by a time integration of Eq. (13) using the explicit Euler method.[26] Figure 2 shows fits for a harmonic potential and for a nonharmonic potential with fourth-order correction. One can see that the pure harmonic model cannot describe the dynamics for increasing pulse lengths. This is due to the change in frequency for higher deflections by a stronger restoring force. The fit with the first nonharmonic correction is in good agreement with the experimental data. The fit parameter for the harmonic potential is $\mu_0 H_{\text{ext}}\lambda = -6.0 \cdot 10^{-11}$ Tm and the fit parameters for the nonharmonic potential are $\mu_0 H_{\text{ext}}\lambda = -7.5 \cdot 10^{-11}$ Tm and $k_2 = 4.5 \cdot 10^{-4}$ $(\text{ns})^{-2}$ $(\text{nm})^{-2}$. For the steeper nonharmonic potential the field has to be

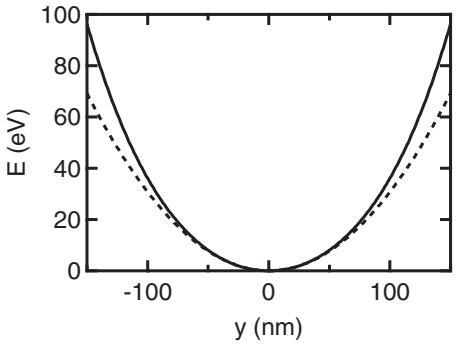

FIG. 3. Harmonic (dashed line) and nonharmonic (solid line) potential deduced from the experimental data.

larger to obtain the same deflection of the domain wall. With this magnitude of the nonharmonic term the harmonic potential holds well for deflections up to 70 nm justifying the harmonic fit for the frequency and the damping. The harmonic and the nonharmonic potential are shown in Fig. 3.

The domain wall width $\lambda = 23$ nm, the domain wall mass $m = 7.6 \cdot 10^{-23}$ kg, and the exciting Oersted field $\mu_0 H_{\text{ext}} = -3.3$ mT are determined in Ref. 11. The domain wall width was determined by using the field dependent deflection of the domain wall. This determination used the potential where we assumed $\alpha = 0.01$. To avoid this assumption in the determination of the damping parameter with Eq. (19) we use the direct imaging of the domain wall to get the wall width. Figure 4 shows the change in contrast depending on the y direction averaged over five pixels in x direction. The inset shows the analyzed area enclosed by yellow lines. The projection of the magnetization along the coordinate axis changes with the Néel wall angle $\theta = \pi - 2 \arctan(e^{(y-Y)/\lambda})$. The magnetization in x direction

$$M_x = M_S \cos\theta = M_S \tanh\left(\frac{y - Y}{\lambda}\right), \tag{21}$$

is fitted to the change in contrast. We obtain a wall width of $\lambda = 24$ nm. This value is in the order of the resolution of the

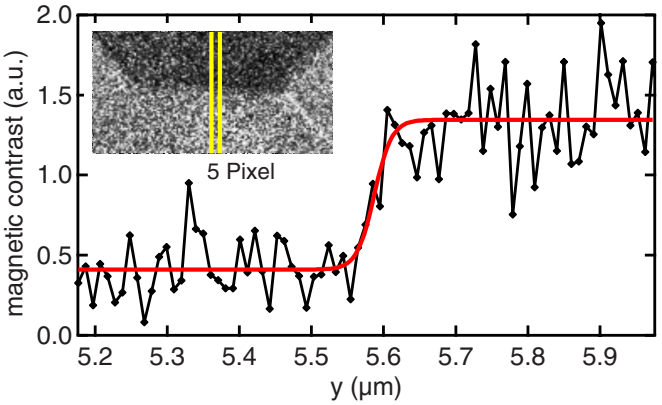

FIG. 4. (Color online) Contrast along the y direction of the section shown in the inset. The value is averaged over five pixels along the x direction. One pixel corresponds to 10 nm. The red line is the magnetization in x direction fitted with Eq. (21).

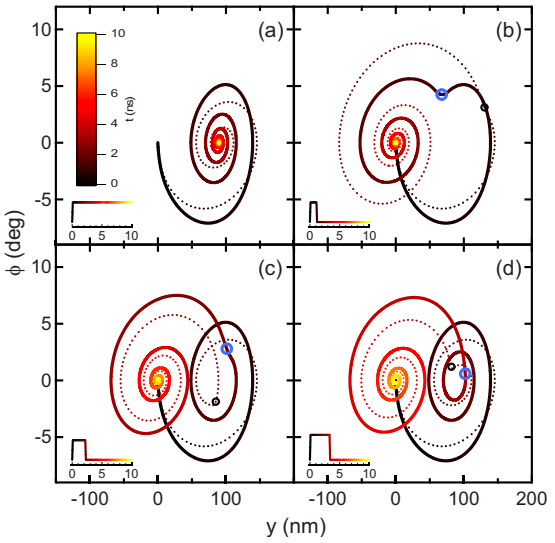

FIG. 5. (Color online) Trajectories in the phase space of position Y and out-of-plane angle ϕ of the domain wall for a steplike field (a) and field pulses of 1.1 (b), 2.2 (c), and 3.3 ns (d). Trajectories for the harmonic and the nonharmonic potential are the dotted and the solid lines, respectively. The color scale indicates the time after the pulse start. The black and blue circles depict the time when the external magnetic field has decreased to half of the amplitude for the harmonic and nonharmonic potential, respectively. The insets depict the pulse profile for the first 10 ns.

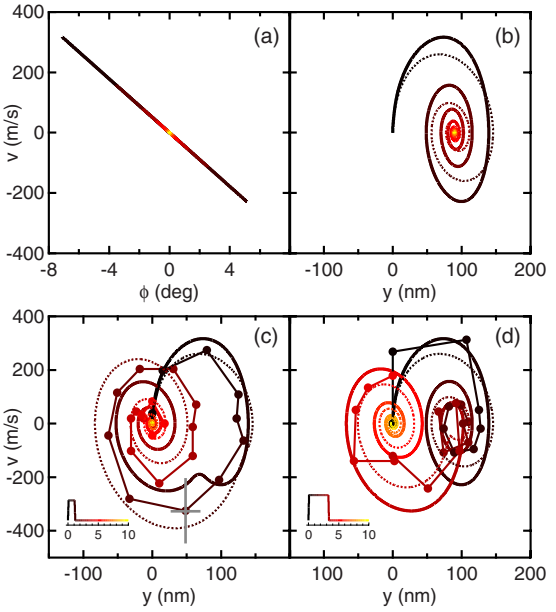

FIG. 6. (Color online) (a) Trajectory in phase space of angle ϕ and velocity v. (b)–(d) Trajectory in phase space of position Y and velocity v. The trajectories in (a) and (b) are for the steplike field [see Fig. 5(a)]. (c) and (d) also show the trajectories observed in the experiment for 1.1 and 3.3 ns long pulses. The lines between the dots are guides to the eye. Trajectories for the harmonic and the nonharmonic potential are the dotted and the solid lines, respectively. The gray lines in (c) depict the error of the data points. Color scale is the same as in Fig. 5.

zone plates used in the experiments. By inserting the result for the domain wall width λ in Eq. (19) we obtain a value of $\alpha=0.0065$.[27] For long domain walls, like the one observed in the experiment, the width is not necessarily constant. Therefore the width does not necessarily reflect the width which has to be used to calculate the anisotropy. However the contribution of $4A/\lambda^2$ in Eq. (19) is small compared to the factor $\mu_0 M_S^2$. Here we avoid any assumption for the damping parameter or for the perpendicular anisotropy. In addition we performed ferromagnetic resonance measurements on permalloy films using a broadband ferromagnetic resonance setup[28] and obtain a damping parameter of $\alpha=0.0064$ in excellent agreement with the above value determined independently via direct imaging of the domain wall oscillation. The values of the damping parameter α are also in good agreement with previous results.[16–21]

A deeper insight into the domain wall oscillation can be gained by visualizing the motion of the domain wall in various phase spaces. The influence of the nonharmonic potential on the, experimentally not observable, out-of-plane tilting angle is studied in this manner. With Eq. (5) we calculate the angle ϕ for our three pulse lengths and for a steplike function with the same amplitude and slope as the field pulses in the experiment for both the harmonic and the nonharmonic potential derived from the fit. The trajectory in the phase space of the position y and the angle ϕ is plotted in Fig. 5. The time zero is set to the point where the pulse starts. In the case of the step function [Fig. 5(a)] the domain wall oscillates to its equilibrium position where the angle ϕ is zero again. For pulsed excitations the domain wall first oscillates around the new equilibrium position and then oscillates back to the old equilibrium position as soon as the pulse is completed. This instantaneous reaction shows that the domain wall mass is not directly linked to the inertial mass of a classical particle. As the LLG equation is a differential equation of first order, the initial velocity of the domain wall does not determine the motion of the domain wall. Only the initial position and the out-of-plane angle of the domain wall determine the temporal evolution.

One can see that the trajectory significantly differs due to the nonharmonic terms. Not only the position of the domain wall changes but also the out-of-plane component, i.e., the angle ϕ, can strongly differ as shown in Fig. 5(b). One can see from Figs. 2(b) and 5(d) that the oscillation due to the pulse of 3.3 ns is resonant in the nonharmonic potential while the oscillation in the harmonic potential is off resonant. For a better understanding of this drastic change in ϕ it is convenient to study different phase spaces depicted in Fig. 6 for the steplike field. Interestingly the angle depends almost perfectly linear on the velocity with negative slope [see Fig. 6(a)] because the second term in Eq. (2) is orders of magnitude smaller than the first term. Then Eq. (2) simplifies to $\dot{Y}=-\frac{\lambda}{\alpha\tau_d}\phi$. Consequently the trajectory in the phase space of position and velocity is inverted along the ordinate in comparison to the one in the phase space of position and angle [compare Figs. 5(a) and 6(b)]. For comparison Figs. 6(c) and 6(d) show the trajectories observed in the experiment and calculated from the model for a 1.1 and 3.3 ns field pulse. The error of the position of the domain wall is only 20 nm but the error in the velocity is up to 117 m/s. Note that the plots in Figs. 6(c) and 6(d) are not suitable to estimate the

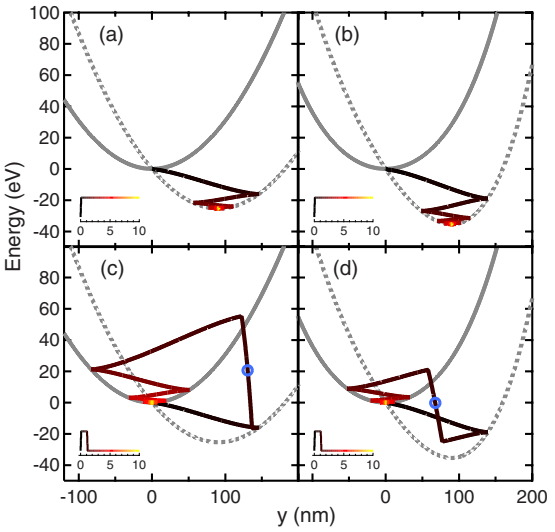

FIG. 7. (Color online) Trajectories in phase space of position and energy for the steplike field (a) and (b) and for a field pulse of 1.1 ns (c) and (d). The trajectories for the harmonic potential (a) and (c) and the nonharmonic potential (b) and (d) are plotted with (dotted line) and without (solid line) applied field. The circles depict the time when the external field has decreased to half of the amplitude. Color scale is the same as in Fig. 5. The insets depict the pulse profile for the first 10 ns.

nonharmonic terms as it has been possible from the domain wall position versus time plot in Fig. 2.

Trajectories in phase space of position and energy are shown in Fig. 7. One can see that the domain wall oscillates with its characteristic damping to the equilibrium position of the potential well with lower potential energy due to the Zeeman contribution. For a pulse length of 1.1 ns the situation differs, the external field disappears and the energy of the domain wall returns to the original potential well. In the harmonic potential shown in Figs. 7(a) and 7(c) the domain wall energy raises to a high potential energy leading to a high kinetic energy in the following. In the nonharmonic potential the domain wall is constrained sooner to the shifted equilibrium position due to the stronger restoring force. Here the domain wall energy is much smaller after the pulse. Hence, the domain wall velocity is smaller and consequently due to the linear dependency its out-of-plane component.

V. CONCLUSION

We presented an analytical model which precisely describes oscillations of a magnetic domain wall in a restoring potential. Nonharmonic terms are introduced to the pinning potential to take deviations from the pure harmonic oscillator model into account. Time resolved x-ray microscopy with high spatial resolution reveals that these nonharmonic terms are necessary to describe the oscillations of a domain wall. Phase space diagrams illustrate the dynamics of the domain wall and show that the behavior of the domain wall is strongly affected by the nonharmonic pinning potential. The damping parameter of permalloy has been determined by a direct imaging method using the domain wall oscillation and is in excellent agreement with ferromagnetic resonance results determined for films.

ACKNOWLEDGMENTS

We thank René Eiselt and Mi-Young Im for collaboration with the x-ray microscope, Toru Matsuyama, Markus Bolte, Daniela Pfannkuche, and Ulrich Merkt for fruitful discussions as well as Sandra Motl for assistance with the analysis of the x-ray images and ferromagnetic resonance measurements. Financial support by the Deutsche Forschungsgemeinschaft via the SFB 668 "Magnetism from the Single Atom to the Nanostructure" and via the Graduiertenkolleg 1286 "Functional Metal-Semiconductor Hybrid Systems" as well as by the city of Hamburg via the cluster of excellence "Nanospintronics" is gratefully acknowledged. The continued support of the staff of CXRO and ALS is highly appreciated. The operation of the soft x-ray microscope is funded by the Director, Office of Science, Office of Basic Energy Sciences, Materials Sciences and Engineering Division, of the U.S. Department of Energy.

*lbocklag@physnet.uni-hamburg.de
†bkrueger@physnet.uni-hamburg.de

[1] S. S. P. Parkin, M. Hayashi, and L. Thomas, Science **320**, 190 (2008).
[2] A. Drews, B. Krüger, G. Meier, S. Bohlens, L. Bocklage, T. Matsuyama, and M. Bolte, Appl. Phys. Lett. **94**, 062504 (2009).
[3] S. Bohlens, B. Krüger, A. Drews, M. Bolte, G. Meier, and D. Pfannkuche, Appl. Phys. Lett. **93**, 142508 (2008).
[4] A. A. Thiele, Phys. Rev. Lett. **30**, 230 (1973).
[5] N. L. Schryer and L. R. Walker, J. Appl. Phys. **45**, 5406 (1974).
[6] B. Krüger, D. Pfannkuche, M. Bolte, G. Meier, and U. Merkt, Phys. Rev. B **75**, 054421 (2007).
[7] B. Krüger, A. Drews, M. Bolte, U. Merkt, D. Pfannkuche, and G. Meier, Phys. Rev. B **76**, 224426 (2007).
[8] M. Kläui, P.-O. Jubert, R. Allenspach, A. Bischof, J. A. C. Bland, G. Faini, U. Rüdiger, C. A. F. Vaz, L. Vila, and C. Vouille, Phys. Rev. Lett. **95**, 026601 (2005).
[9] M. Hayashi, L. Thomas, C. Rettner, R. Moriya, and S. S. P. Parkin, Nat. Phys. **3**, 21 (2007).
[10] G. Meier, M. Bolte, R. Eiselt, B. Krüger, D.-H. Kim, and P. Fischer, Phys. Rev. Lett. **98**, 187202 (2007).
[11] L. Bocklage, B. Krüger, R. Eiselt, M. Bolte, P. Fischer, and G. Meier, Phys. Rev. B **78**, 180405(R) (2008).
[12] O. Boulle, L. Heyne, J. Rhensius, M. Kläui, U. Rüdiger, L. Joly, L. Le Guyader, F. Nolting, L. J. Heyderman, G. Malinowski, H. J. M. Swagten, B. Koopmans, C. Ulysse, and G. Faini, J. Appl. Phys. **105**, 07C106 (2009).
[13] M. Bolte, G. Meier, B. Krüger, A. Drews, R. Eiselt, L. Bocklage, S. Bohlens, T. Tyliszczak, A. Vansteenkiste, B. Van Waeyenberge, K. W. Chou, A. Puzic, and H. Stoll, Phys. Rev. Lett. **100**,

176601 (2008).
[14] W. Chao, B. D. Harteneck, J. A. Liddle, E. H. Anderson, and D. T. Attwood, Nature (London) **435**, 1210 (2005).
[15] A. Puzic, B. Van Waeyenberge, K. W. Chou, P. Fischer, T. Tyliszczak, K. Rott, H. Brückl, G. Reiss, I. Neudecker, T. Haug, M. Buess, and C. H. Back, J. Appl. Phys. **97**, 10E704 (2005).
[16] S. Ingvarsson, L. Ritchie, X. Y. Liu, G. Xiao, J. C. Slonczewski, P. L. Trouilloud, and R. H. Koch, Phys. Rev. B **66**, 214416 (2002).
[17] M. Bailleul, D. Olligs, and C. Fermon, Appl. Phys. Lett. **83**, 972 (2003).
[18] D. J. Twisselmann and R. D. McMichael, J. Appl. Phys. **93**, 6903 (2003).
[19] S. Tamaru, J. A. Bain, R. J. M. van de Veerdonk, T. M. Crawford, M. Covington, and M. H. Kryder, Phys. Rev. B **70**, 104416 (2004).
[20] M. L. Schneider, T. Gerrits, A. B. Kos, and T. J. Silva, Appl. Phys. Lett. **87**, 072509 (2005).
[21] S. S. Kalarickal, P. Krivosik, M. Wu, C. E. Patton, M. L. Schneider, P. Kabos, T. J. Silva, and J. P. Nibarger, J. Appl. Phys. **99**, 093909 (2006).
[22] W. Döring, Z. Naturforsch. A **3a**, 373 (1948).
[23] L. Thomas, M. Hayashi, X. Jiang, R. Moriya, C. Rettner, and S. S. P. Parkin, Nature (London) **443**, 197 (2006).
[24] D. Bedau, M. Kläui, M. T. Hua, S. Krzyk, U. Rüdiger, G. Faini, and L. Vila, Phys. Rev. Lett. **101**, 256602 (2008).
[25] C. T. Chen, F. Sette, Y. Ma, and S. Modesti, Phys. Rev. B **42**, 7262 (1990).
[26] We use $\alpha=0.01$ for permalloy.
[27] With $M_S=8.6\cdot10^5$ A/m and $A=1.3\cdot10^{-11}$ J/m.
[28] J. Podbielski, F. Giesen, and D. Grundler, Phys. Rev. Lett. **96**, 167207 (2006).